JCTC Journal of Chemical Theory and Computation

Article

pubs.acs.org/JCTC

Energy-Specific Equation-of-Motion Coupled-Cluster Methods for High-Energy Excited States: Application to *K*-edge X-ray Absorption Spectroscopy

Bo Peng,[†] Patrick J. Lestrange,[†] Joshua J. Goings,[†] Marco Caricato,[‡] and Xiaosong Li*[,†]

[†]Department of Chemistry, University of Washington, Seattle, Washington 98195, United States

[‡]Department of Chemistry, University of Kansas, Lawrence, Kansas 66045, United States

Supporting Information

ABSTRACT: Single-reference techniques based on coupled-cluster (CC) theory, in the forms of linear response (LR) or equation of motion (EOM), are highly accurate and widely used approaches for modeling valence absorption spectra. Unfortunately, these equations with singles and doubles (LR-CCSD and EOM-CCSD) scale as $O(N^6)$, which may be prohibitively expensive for the study of high-energy excited states using a conventional eigensolver. In this paper, we present an energy-specific non-Hermitian eigensolver that is able to obtain high-energy excited states (e.g., XAS *K*-edge spectrum) at low computational cost. In addition, we also introduce an improved trial vector for iteratively solving the EOM-CCSD equation with a focus on high-energy eigenstates. The energy-specific EOM-CCSD approach and its low-scaling alternatives are applied to calculations of carbon, nitrogen, oxygen, and sulfur *K*-edge excitations. The results are compared to other implementations of CCSD for excited states, energy-specific linear response time-dependent density functional theory (TDDFT), and experimental results with multiple statistical metrics are presented and evaluated.

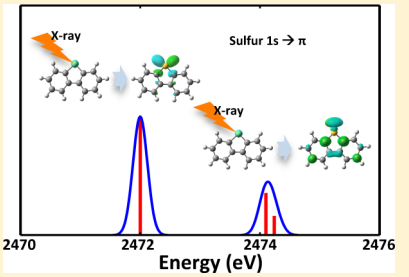

1. INTRODUCTION

Advances in laser light sources have made X-ray absorption spectroscopy (XAS) a powerful tool in modern day chemical research. In XAS, excitations of core electrons to either weakly bound or continuum states can be used to characterize the electronic and molecular structure of a chemical or material system.[1] Excitations to bound states provide information about the valence electronic structure, while the scattering of the photoelectrons generated by excitation to continuum states provides information about the molecular geometry. The ability to simultaneously probe both electronic and nuclear degrees of freedom has made XAS an irreplaceable tool in the fields of surface science[1−3] and inorganic catalysis.[4−6]

Because of its complexity, XAS often relies on theoretical insight for interpretation. As in lower energy absorption spectroscopy, variants of time-dependent density functional theory (TDDFT)[7−9] are the most frequently used methods. The restricted excitation window (REW-TDDFT)[10−13] and energy-specific (ES-TDDFT)[13−15] TDDFT approaches are now routinely used to model XAS. The REW-TDDFT method restricts solutions to only include transitions from orbitals deemed relevant to a particular region of the spectrum, whereas the ES-TDDFT approach searches for solutions in the full orbital space with a constraint on the eigenvalues. These two different numerical approaches have been shown to produce almost identical X-ray *K*-edge spectra because excitations from the 1*s* (*K*-edge) orbital are rather localized in the orbital space.[16] Variations of the ΔSCF approach,[17] such as the transition-potential DFT[18,19] and the orthogonality constrained DFT,[20,21] which require the preparation of a core−hole single determinant state, have been successfully applied to XAS. From the DFT kernel perspective, there has also been interest in developing short-range corrected functionals that improve the description of core correlation and reduce the self-interaction error specifically for XAS.[22,23]

Wave-function-based approaches, while more expensive, are inherently free of the self-interaction error and can be systematically improved. For example, single-reference techniques based on coupled-cluster (CC) theory, in the forms of linear response (LR)[24,25] or equation of motion (EOM),[26,27] are highly accurate and widely used approaches for modeling valence absorption spectra.[28,29] Unfortunately, these equations with singles and doubles (LR-CCSD and EOM-CCSD) scale as $O(N^6)$, which may be prohibitively expensive for the study of large molecular systems. This high computational cost has prompted the development of many low-scaling approximations to EOM-CCSD and LR-CCSD. The EOM-MBPT2 equation is obtained by truncating the perturbative expansion of the cluster operator at second order.[30,31] This approach still scales as $O(N^6)$ but with a much smaller prefactor than that of EOM-CCSD. Partitioned EOM-MBPT2 (P-EOM-MBPT2) is an iterative $O(N^5)$ approach that makes the further approximation that the doubles−doubles block of the Hamiltonian can be treated as diagonal.[31−33] While these

Received: May 18, 2015

DOI: 10.1021/acs.jctc.5b00459
J. Chem. Theory Comput. XXXX, XXX, XXX−XXX

techniques have been extensively used in obtaining low-lying excited states, they have not been applied to the study of core excitations, although further approximations to these techniques have been used previously with varying success.

Beyond coupled cluster, there are other wave function and Green's function based methods to study high-energy excited states. The CIS(D_∞) approach can be related to P-EOM-MBPT2 by treating the singles−doubles blocks of the Hamiltonian to first-order only.[34] The second-order algebraic-diagrammatic construction approach (ADC(2)) is a symmetrized form of CIS(D_∞) that has been previously used to model XAS.[35−37] The core valence separation approximation (CVS)[38] is employed to reduce the dimension of the problem by only including excitations from the relevant core orbitals; however, there is an estimated 0.5−1.0 eV error associated with the CVS approximation.[36] The closely related CIS(D) method applies a noniterative doubles correction to excitation energies obtained from configuration interaction singles (CIS).[39,40] By using the REW approach, CIS(D) can be used to model core excitations, but has been known to provide qualitatively incorrect spectra in some cases.[41]

Where core excitations are concerned, direct applications of EOM-CCSD and its closely related derivatives are computationally intractable, because of the large space where the excited states of interest reside. The electron-attachment EOM-CCSD (EA-EOM-CCSD)[42] has been used previously to investigate *K*-edge transitions in small molecules, relying on the validity and availability of a core−hole reference state. Recently, an equation-of-motion multireference coupled-cluster including singles and doubles (EOM-MRCCSD) has been developed to obtain core excitations in the coupled-cluster framework.[43−45] The EOM-MRCCSD approach for XAS is based on the construction of a core−hole reference in a select subspace spanned by active core, occupied, and unoccupied spin−orbitals of interest. Recently, a complex polarization propagator formulation of coupled-cluster response theory (CPP-CC) has been applied to model X-ray absorption among other properties.[46−48] This formalism can be used for many different coupled-cluster approaches truncated at different levels (CCS, CC2, CCSD, CCSD(3)). Unlike EOM-CC, which solves for resonant frequencies or poles of the response function, the CPP-CC method solves a damped frequency-dependent response function. This technique is able to resolve the off-resonant response of the system, but requires the solution of many frequency-dependent problems.

In this paper, we present an energy-specific non-Hermitian eigensolver with improved trial vectors to efficiently solve the EOM-CCSD equation for high-energy core excitations. This approach utilizes low-scaling approximations of EOM-CCSD to refine trial vectors, followed by iterative eigenvalue-screening, eigenvector-bracketing, and growing window techniques to search for high-energy solutions in the full orbital space. The strategy used throughout is a non-Hermitian generalization of our previously developed energy-specific algorithm applied in TDDFT.[14] This strategy will allow these highly accurate single-reference wave function methods to be routinely applied to the study of core excitations.

2. METHOD

2.1. Brief Review of EOM-CCSD, EOM-MBPT2, and P-EOM-MBPT2. For two excellent articles of coupled cluster theory, see the review by Crawford and Schaefer[49] and the book by Shavitt and Bartlett.[29] In the present work, we adopt the notation that indices *i*, *j*, *k*, *l* refer to occupied orbitals, *a*, *b*, *c*, *d* refer to virtual orbitals, and *p*, *q*, *r*, *s* refer to any orbital.

The generalized CC Schrödinger equation may be written as

$$\bar{H}\hat{R}(m)|\Phi_0\rangle = E_m\hat{R}(m)|\Phi_0\rangle \tag{1}$$

where $|\Phi_0\rangle$ is the reference wave function, and $\hat{R}(m)$ is the excitation operator for the *m*th excited state with energy E_m. This takes the form

$$\begin{aligned}\hat{R}(m) &= \hat{R}_1 + \hat{R}_2 + \ldots \\ &= \sum_{ia} r_i^a(m)a_a^\dagger a_i + \sum_{\substack{i<j\\a<b}} r_{ij}^{ab}(m)a_a^\dagger a_b^\dagger a_j a_i + \ldots\end{aligned} \tag{2}$$

where $a^\dagger$ and a are creation and annihilation operators. $\bar{H}$ is the similarity transformation of the bare electronic Hamiltonian $\hat{H}$,

$$\bar{H} = e^{-\hat{T}}\hat{H}e^{\hat{T}} \tag{3}$$

in which the cluster operator $\hat{T}$ takes the following form,

$$\hat{T} = \hat{T}_1 + \hat{T}_2 + \ldots = \sum_{ia} t_i^a a_a^\dagger a_i + \frac{1}{4}\sum_{ijab} t_{ij}^{ab} a_a^\dagger a_b^\dagger a_j a_i + \ldots \tag{4}$$

Equation 1 represents a right-hand eigenvalue problem; however, eq 3 makes $\bar{H}$ non-Hermitian. As a result, eq 1 is different from its associated left-hand eigenvalue problem,

$$\langle\Phi_0|\hat{L}(m)\bar{H} = \langle\Phi_0|\hat{L}(m)E_m \tag{5}$$

where $\hat{L}(m)$ is the de-excitation operator, which is defined as

$$\begin{aligned}\hat{L}(m) &= \hat{L}_1 + \hat{L}_2 + \ldots \\ &= \sum_{ia} l_a^i(m)a_i^\dagger a_a + \sum_{\substack{i<j\\a<b}} l_{ab}^{ij}(m)a_i^\dagger a_j^\dagger a_b a_a + \ldots\end{aligned} \tag{6}$$

Note that eqs 1 and 5 share the same eigenvalues (E_m) and the left-hand and right-hand eigenvectors are related to each other through the biorthonormality condition,

$$\langle\Phi_0|\hat{L}(m)\hat{R}(n)|\Phi_0\rangle = \delta_{m,n} \tag{7}$$

such that the generalized CC energy expression can be obtained:

$$E_m = \langle\Phi_0|\hat{L}(m)\bar{H}\hat{R}(m)|\Phi_0\rangle \tag{8}$$

In order to calculate electronic excitation energies, it is convenient to define a normal-ordered Hamiltonian, $\bar{H}_N$, by

$$\bar{H}_N = \bar{H} - E_0 \tag{9}$$

where E_0 is the energy associated with ground-state wave function $|\Phi_0\rangle$. Then, eq 8 can be rewritten as

$$\omega_m = \langle\Phi_0|\hat{L}(m)\bar{H}_N\hat{R}(m)|\Phi_0\rangle \tag{10}$$

where ω_m is the *m*th excitation energy out of the ground state.

Within the framework of the EOM-CCSD method, $\hat{L}$ and $\hat{R}$ are truncated to the second order, the excitation energies are obtained by diagonalizing the EOM-CCSD Hamiltonian matrix,

DOI: 10.1021/acs.jctc.5b00459
J. Chem. Theory Comput. XXXX, XXX, XXX−XXX

$$\mathbf{H}_{\text{EOM-CCSD}} = \begin{bmatrix} \bar{H}^{\text{SS}} & \bar{H}^{\text{SD}} \\ \bar{H}^{\text{DS}} & \bar{H}^{\text{DD}} \end{bmatrix}$$
$$\bar{H}^{\text{SS}}_{ai,ck} = \langle \Phi_i^a | \bar{H}_N | \Phi_k^c \rangle$$
$$\bar{H}^{\text{SD}}_{ai,cdkl} = \langle \Phi_i^a | \bar{H}_N | \Phi_{kl}^{cd} \rangle$$
$$\bar{H}^{\text{DS}}_{abij,ck} = \langle \Phi_{ij}^{ab} | \bar{H}_N | \Phi_k^c \rangle$$
$$\bar{H}^{\text{DD}}_{abij,cdkl} = \langle \Phi_{ij}^{ab} | \bar{H}_N | \Phi_{kl}^{cd} \rangle \quad (11)$$

where $|\Phi_k^c\rangle$, $|\Phi_{kl}^{cd}\rangle$ are singly and doubly excited determinants, respectively. The overall dimension of eq 11 is $OV + O^2V^2$, where O and V are the numbers of occupied and virtual orbitals. EOM-CCSD scales as $O(N^6)$ and a lower scaling approximation can be obtained by only keeping terms in the perturbative expansion of the cluster operator through second order. This gives rise to the EOM-MBPT2 Hamiltonian matrix,[30,32,33]

$$\mathbf{H}_{\text{EOM-MBPT2}} = \begin{bmatrix} \bar{H}^{\text{SS}(2)} & \bar{H}^{\text{SD}(2)} \\ \bar{H}^{\text{DS}(2)} & \bar{H}^{\text{DD}(2)} \end{bmatrix} \quad (12)$$

where $\bar{H}^{\text{SS}(2)}$ is the singles−singles block of the Hamiltonian, $\bar{H}^{\text{SS}}$, through second order, and so on. This approximation neglects the numerous $\hat{T}_1$ terms, as $\hat{T}_1^{(1)}$ equals zero in the perturbative approach, and only needs the $\hat{T}_2^{(1)}$ amplitudes, which are determined through

$$t_{ij}^{ab(1)} = \frac{\langle ij||ab\rangle}{\epsilon_i + \epsilon_j - \epsilon_a - \epsilon_b} \quad (13)$$

where the ϵ terms are the Hartree−Fock molecular orbital energies.

EOM-MBPT2 is still a $O(N^6)$ method, but with a much smaller prefactor than EOM-CCSD. Further approximation can be made by replacing $\bar{H}^{\text{DD}(2)}$ with its zeroth order based on the Löwdin partitioning approach[50] to give rise to an iterative $O(N^5)$ method, the so-called "partitioned EOM-MBPT2" (P-EOM-MBPT2).[32,33,50] The P-EOM-MBPT2 Hamiltonian is

$$\mathbf{H}_{\text{P-EOM-MBPT2}} = \begin{bmatrix} \bar{H}^{\text{SS}(2)} & \bar{H}^{\text{SD}(2)} \\ \bar{H}^{\text{DS}(2)} & \bar{H}^{\text{DD}(0)} \end{bmatrix} \quad (14)$$

where $\bar{H}^{\text{DD}(0)} = \epsilon_a + \epsilon_b - \epsilon_i - \epsilon_j$.

In practice, because of the non-Hermitian nature of Hamiltonians in eqs 11, 12, and 14, and their large matrix dimension (roughly O^2V^2, with O and V being the numbers of occupied and virtual orbitals), the most efficient computational approach to find the lowest eigenvalues and corresponding left and right eigenvectors is a modified version of the Davidson algorithm.[51−54] However, core excitations in XAS usually exhibit high excitation energies ranging from hundreds to thousands of electron volts, and are thus far away from low-lying excited states. It is then impractical for the conventional EOM methods mentioned above to capture these high energy excited states, because ordinary solvers require that all lower-energy solutions be obtained before any higher-energy solution.

2.1.1. Improved Trial Vectors for High-Energy Excited States. Davidson-like eigensolvers usually initialize with a set of well-defined guess vectors, and the quality of these guess vectors subsequently affects the convergence speed in iterative methods for eigenvalue problems. In TDDFT, trial vectors constructed from simple occupied to virtual orbital transitions have proven to be quite reasonable. However, such trial vectors are usually far from the converged EOM-CCSD solution and, as a result, they may lead to excessive iterations with Davidson-like eigensolvers. A better and widely used trial vector scheme for EOM-CCSD in practice starts with the solution of configuration interaction singles (CIS). However, generating trial vectors for high-energy excited states using conventional CIS calculations is impractically expensive with conventional techniques. As a result, the feasibility of applying EOM-CCSD approach for XAS calculations is dependent on the availability of appropriate trial vectors and efficient solvers that can obtain the high-energy eigenvectors of interest. In this work, we develop a two-step strategy to generate appropriate trial vectors that aims to enable EOM-CCSD and its low-scaling approximations to study high-energy excitations such as those probed by XAS.

Assume that M excited states with energies greater than ω_0 are the subject of interest to be investigated using EOM-CCSD. In the first step, high-energy trial vectors are generated using the energy-specific eigensolvers with low-scaling excited state methods such as CIS and P-EOM-MBPT2. For CIS, the Hermitian energy-specific algorithm[14] is used to obtain m eigenvectors ($m \geq M$, $\omega \geq \omega_0$) as trial vectors for the following calculation. As the CIS approach does not have electron correlation, their eigenvectors can be poor guesses for high-energy excited states as contributions from $\hat{T}_2$ become more important.[31] In fact, in our test cases, searching for high-energy eigenvectors in the EOM-CCSD framework usually takes many more iterations, compared to those for valence excitations. Any improvement to expedite solving the EOM-CCSD equations for high-energy excited states will be appreciated.

To improve the CIS vectors for high-energy EOM-CCSD calculations, we introduce a second step to refine the trial vectors using the $O(N^5)$ P-EOM-MBPT2 approach with a non-Hermitian energy-specific eigensolver, which will be introduced later in this paper. The refined trial vectors will be used together with the non-Hermitian energy-specific eigensolver to obtain solutions of the EOM-CCSD equation. In the following discussion, methods that utilize the energy-specific eigensolver (Hermitian or non-Hermitian) will have the "ES-" prefix in order to distinguish the results from those using conventional algorithms.

Figure 1 shows the effect of the quality of different trial vectors on the convergence behavior of an ES-EOM-CCSD calculation of a carbon K-edge excitation of CO. Two different tight convergence criteria are considered in this comparison: the residual norm and the change in excitation energy. For both criteria, EOM-CCSD using the P-EOM-MBPT2 eigenvectors as trial vectors exhibits a savings of ∼20% in computational cost. Note that the cost of computing ES-P-EOM-MBPT2 eigenvectors is trivial, compared to the cost of solving the $O(N^6)$ EOM-CCSD equation. This test case suggests that P-EOM-MBPT2 eigenvectors are a better choice over the CIS trial vectors for ES-EOM-CCSD calculations.

2.2. Non-Hermitian Energy-Specific Eigensolver. In this work, we introduce a non-Hermitian energy-specific eigensolver for EOM-CCSD and its low-scaling approximations to efficiently compute high-energy excited states. The discussion starts with a set of left $\mathbf{L} = \{L_1, ..., L_m\}$ and right $\mathbf{R} = \{R_1, ..., R_m\}$ trial vectors in the full orbital space that

DOI: 10.1021/acs.jctc.5b00459
J. Chem. Theory Comput. XXXX, XXX, XXX−XXX

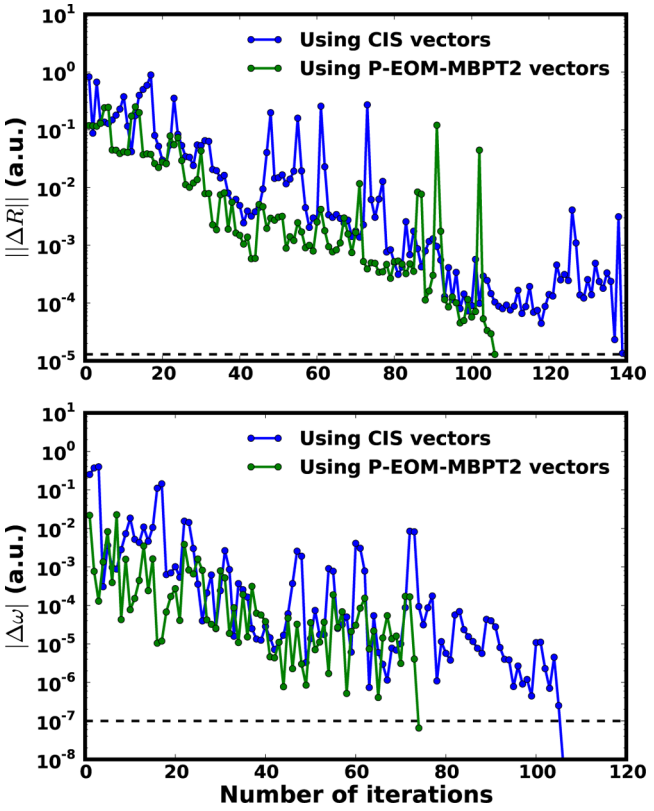

Figure 1. Comparison of the convergence behaviors of ES-EOM-CCSD calculations using CIS and P-EOM-MBPT2 trial vectors for the C 1*s* → 2*pπ** transition of CO. The residual norm of the right eigenvector (top panel) and the absolute change of eigenvalues (bottom panel) are plotted against the number of iterations. The basis set used is 6-311G**, and the calculated excitation energy is 288.32 eV.

correspond to initial guesses of high-energy excited states generated using the two-step strategy presented above. Note that the left and right vectors are related by the biorthonormalization condition eq 7. The EOM Hamiltonian **H** (eq 11) is projected onto the subspace spanned by the trial vectors,

$$\mathbf{h} = \mathbf{L}^{\dagger}\mathbf{H}\mathbf{R} \tag{15}$$

The EOM Hamiltonian in the reduced space **h** is then diagonalized to obtain a new set of left $\mathbf{l} = \{l_1, ..., l_m\}$ and right $\mathbf{r} = \{r_1, ..., r_m\}$ eigenvectors and eigenvalues $\omega = \{\omega_1, ..., \omega_m\}$. Eigenpairs in the reduced space are screened and only the ones with associated eigenvalues above the desired energy threshold ω_0 are kept. The transformation of these qualified eigenpairs from the reduced space to the full orbital space yields the new approximate eigenvectors,

$$\tilde{\mathbf{R}} = \mathbf{R}\mathbf{r},\ \tilde{\mathbf{L}} = \mathbf{L}\mathbf{l} \tag{16}$$

Equation 7 is used to ensure that the new left and right eigenvectors are biorthonormalized. To test the convergence, the eigenvector residuals of states of interest are computed:

$$\Delta R_k = (\mathbf{H} - \mathbf{I}\omega_k)R_k \tag{17}$$

$$\Delta L_k = (\mathbf{H}^{\dagger} - \mathbf{I}\omega_k)L_k \tag{18}$$

If some of the norms of residuals are still above the predefined threshold, perturbation vectors are generated using the following equation:

$$R'_k = (\mathbf{I}\omega_k - \mathbf{H}_{\mathrm{D}})^{-1}\Delta R_k \tag{19}$$

$$L'_k = (\mathbf{I}\omega_k - \mathbf{H}_{\mathrm{D}})^{-1}\Delta L_k \tag{20}$$

where $\mathbf{H}_{\mathrm{D}}$ are the diagonal elements of the **H** matrix.[51,52] In our implementation, as in previous studies,[53,55] $\mathbf{H}_{\mathrm{D}}$ is approximated by the corresponding orbital energy differences. The perturbation vectors are biorthonormalized and added to **R** and **L** to form the new subspace for the next iteration starting from eq 15. If complex eigenvalues are obtained in the intermediate iteration, the space of **R** and **L** must be increased. The larger number of expansion vectors can not only benefit the elimination of complex eigenvalues, but also help to accelerate the convergence.[8,53] This process is repeated until the norm of the residuals is below the desired threshold.

The two-step calculation strategy and energy-screening and eigenvector-bracketing technique introduced above avoids the scan through low-lying excited states in EOM calculations, while improving the quality of trial vectors for EOM-CCSD calculation by using converged eigenvectors associated with the high-energy excited states from low-scaling EOM calculations. This makes it possible to calculate high-energy excited states with coupled-cluster theory.

3. BENCHMARKS AND DISCUSSION

Energy-specific variations of EOM-CCSD, EOM-MBPT2, and P-EOM-MBPT2 have been implemented and tested in a development version of the Gaussian software package.[56] For all excited-state calculations, the convergence is obtained when (i) the norm of the residual vectors is below a threshold, 10^{-5} a.u., as recommended by Stanton and Bartlett;[26] or (ii) the change in the eigenvalues is $<10^{-7}$ a.u.[53] All ground-state geometries were optimized at the CCSD level with the def2-TZVPD basis set.[57−60]

As discussed in the Methods section, the energy-specific eigensolver is able to obtain the exact solutions represented in the full space. This has been verified by benchmark calculations on select excited states using the ES-EOM-CCSD method, compared to those obtained by full EOM-CCSD calculations including low-lying states. In Table 1, the results from ES-EOM-CCSD and EOM-CCSD are numerically identical, suggesting that the energy-specific approach is able to obtain the exact excited states even though low-lying states are not considered in the eigenvector search algorithm. Since the full EOM-CCSD calculation must include extra low-lying states in order to locate the states in the targeted energy range, it unavoidably incurs additional 2-fold computational cost, compared to the ES-EOM-CCSD method in this test case. Assuming that the number of excited states (i.e., the number of **R** and **L** vectors) grows linearly, with respect to the excitation

Table 1. Comparison of Conventional EOM-CCSD and ES-EOM-CCSD for Select Low-Lying Excited States of Carbon Monoxide Computed with the def2-TZVPD Basis Set[a]

		Energy (eV)	
state	transition	ES-EOM-CCSD	EOM-CCSD
$B^1\Sigma^+$	$\sigma \rightarrow 3s$	11.27	11.27
$C^1\Sigma^+$	$\sigma \rightarrow 3p\sigma$	12.30	12.30
$E^1\Pi$	$\sigma \rightarrow 3p\pi$	12.32	12.32
$F^1\Sigma^+$	$\sigma \rightarrow 3d\sigma$	13.53	13.53

[a]The energy threshold for the energy-specific calculations is 11.2 eV.

DOI: 10.1021/acs.jctc.5b00459
J. Chem. Theory Comput. XXXX, XXX, XXX−XXX

energy, the computational cost of each EOM-CCSD iteration will grow linearly, with respect to the energy of the targeted states. For core−electron excitations, the cost of the conventional EOM-CCSD approach becomes intractable. In contrast, the computational cost of ES-EOM-CCSD is almost constant, because, in principle, the search space is invariant to the excitation energy range of interest.

The quality of the ES-EOM-CCSD approach is also compared to other implementations/approximations of CC method to XAS. Table 2 compares oxygen *K*-edge excitations of H_2O obtained using ES-EOM-CCSD to those computed using multireference EOM-MRCCSD[43−45] and single-reference CPP-CCSD.[61] Table 3 shows ES-EOM-CCSD and EA-EOM-CCSD[42] results for *K*-edge excitations of a select test set. This comparison shows that, for the limited number of test cases, ES-EOM-CCSD results are in excellent agreement with the results from other coupled-cluster methods. The difference between ES-EOM-CCSD and EA-EOM-CCSD can be attributed to the different reference used in the calculation. The EA-EOM-CCSD method requires a predefined core−hole reference that accounts for some amount of core−hole relaxation. Therefore, the EA-EOM-CCSD results can be of higher accuracy, although they are strongly dependent on the quality and existence of the core−hole reference.

Table 2. Comparison of ES-EOM-CCSD with the Multireference EOM-MRCCSD[43−45] Method and the Single-Reference CPP-CCSD[61] Method for Select Core Excitations of H_2O

basis	Energy (eV) ES-EOM-CCSD	EOM-MRCCSD	CPP-CCSD[a]	experiment[b]
	$1a_1 \rightarrow 4a_1$ Excitation			
6-311G**	535.72	535.76[c]		534.00
cc-pVDZ	538.36	538.40[c,d]		
cc-pVTZ	535.41	535.34[d]		
aug-cc-pVTZ	535.30	535.32[e]		
aug-cc-pCVTZ	535.66		535.68	
	$1a_1 \rightarrow 2b_1$ Excitation			
6-311G**	537.57	537.61[c]		535.90
cc-pVDZ	540.17	540.21[c,d]		
cc-pVTZ	537.22	537.13[d]		
aug-cc-pVTZ	537.08	537.11[e]		
aug-cc-pCVTZ	537.44		537.47	

[a]Data taken from ref 61. [b]Data taken from ref 62. [c]Data taken from ref 43. [d]Data taken from ref 44. [e]Data taken from ref 45.

Excitation energies of a set of 31 *K*-edge transitions for carbon, nitrogen, and oxygen, of seven molecules (CO, CH_2O, C_2H_4, N_2, NH_3, NO_2, H_2O) are calculated with ES-EOM-CC methods (see Supporting Information for details). The results are compared with results from gaseous XAS or inner-shell electron energy loss spectroscopy (ISEELS) experiments.[62,66,70−74] The mean absolute/signed error (MAE/MSE), root-mean-square (RMS) error, maximum absolute error (Max AE), mean standard error (MSE), and standard deviation (StDev) of the errors, with respect to experimental results are statistically evaluated. Energy-specific TDDFT (ES-TDDFT)[14] results are also included for comparison. Two density functionals, BHandHLYP[75] and PBE1PBE[76,77] were used, since they have been shown to perform consistently well for predicting *K*-edge spectra.[15]

Table 3. Comparison of ES-EOM-CCSD with EA-EOM-CCSD for Select Core Excitations[a]

molecule	core	excitation	ES-EOM-CCSD	EA-EOM-CCSD[b]	experiment
CO	carbon	$2\sigma \rightarrow 2\pi$	287.99	287.08	287.40[c]
	oxygen	$1\sigma \rightarrow 2\pi$	535.52	534.15	534.21[d]
C_2H_2	carbon	$1\sigma_u \rightarrow 1\pi_g(2p)$	286.70	286.21	285.81[e]
C_2H_4	carbon	$1b_{1u} \rightarrow 1b_{2g}(2p)$	285.87	285.16	284.87[e]
N_2	nitrogen	$1\sigma_u \rightarrow 1\pi_g$	401.93	401.73	401.00[f]
CH_2O	carbon	$2a_1 \rightarrow 2b_1(\pi^*)$	287.57	285.77	286.00[d]
	oxygen	$1a_1 \rightarrow 2b_1(\pi^*)$	532.43	530.78	530.80[d]

[a]The EA-EOM-CCSD results are based on pre-defined core-hole reference states, and the latter is obtained from a so-called quasi-RHF (QRHF) calculation.[63−65] A modified Sadlej basis set is used in both calculations, where some atomic *s* and *p* functions are uncontracted from the original Sadlej basis set (see ref 42 for more details). [b]Data taken from ref 42. [c]Data taken from ref 66. [d]Data taken from ref 67. [e]Data taken from ref 68. [f]Data taken from ref 69.

Table 4 lists the error analyses of absolute and shifted *K*-edge excitation energies (300−500 eV for these systems) obtained with different methods and the doubly augmented Dunning basis with flexible core orbitals (d-aug-cc-pCVDZ).[78,79] While the absolute excitation energies are a direct measurement of the accuracy of a method, uniform shifts are often applied to calculated XAS to account for the lack of relativistic effects and higher-order correlations.[12,80,81] For error analyses of shifted results, the calculated excitation energies are uniformly shifted so that the lowest energy transition matches the corresponding experimental value. Errors are calculated using the remaining transitions.

DFT methods (BHandHLYP and PBE1PBE) consistently underestimate absolute *K*-edge excitation energies, whereas wave-function-based methods overestimate the *K*-edge excitations. The ES-BHandHLYP method surprisingly outperforms even ES-EOM-CCSD. This is due to fortuitous error cancellation in the BHandHLYP functional, which includes 50% HF exchange, which shifts the spectra to the opposite sign compared to those from pure functionals.[15] For details regarding the performance of ES-TDDFT on XAS calculations, we refer the reader to ref 15.

After the *K*-edge excitation energies are shifted, the associated errors change significantly. All methods considered herein become more reliable with MAEs of <1 eV with a standard deviation of <0.5 eV. ES-EOM-CCSD shows the best performance in all statistical metrics. It consistently overestimates *K*-edge excitation energies only by 0.2−0.3 eV. The lower-scaling alternatives of ES-EOM-CCSD, as represented by ES-EOM-MBPT2 and ES-P-EOM-MBPT2, also show a consistent overestimation with slightly larger errors, yet still outperform DFT-based methods. Note that the difference between these low-scaling methods and ES-EOM-CCSD is much greater for these core excitations than for valence and Rydberg excitations.[31] Although inclusion of triples has shown

DOI: 10.1021/acs.jctc.5b00459
J. Chem. Theory Comput. XXXX, XXX, XXX−XXX

Table 4. Error Analyses of Calculated 31 *K*-edge Excitation Energies (eV)[a]

	Absolute *K*-edge Excitation Energy (eV)				Shifted *K*-edge Excitation Energy (eV)			
	mean absolute error, MAE (StDev)[b]	mean signed error, MSE (StDev)[b]	root mean square, RMS	maximum absolute error, Max AE	mean absolute error, MAE (StDev)[b]	mean signed error, MSE (StDev)[b]	root mean square, RMS	maximum absolute error, Max AE
ES-PBE1PBE	11.68 (1.35)	−11.68 (1.35)	11.75	14.17	0.95 (0.42)	−0.95 (0.42)	1.04	1.67
ES-BHandHLYP	1.99 (0.61)	−1.99 (0.61)	2.08	3.58	0.62 (0.38)	0.45 (0.58)	0.72	1.49
ES-P-EOM-MBPT2	5.24 (0.66)	5.24 (0.66)	5.28	6.92	0.49 (0.34)	−0.18 (0.58)	0.59	1.19
ES-EOM-MBPT2	3.42 (0.57)	3.42 (0.57)	3.46	4.80	0.29 (0.29)	0.23 (0.34)	0.41	0.86
ES-EOM-CCSD	3.11 (0.53)	3.11 (0.53)	3.15	4.37	0.27 (0.26)	0.20 (0.32)	0.37	0.76

[a]For error analyses of shifted energies, excitation energies are uniformly shifted so that the lowest energy transition matches the corresponding experimental value. ES-TDDFT results were obtained using the method described in ref 14, and the basis set used is d-aug-cc-pCVDZ. [b]StDev denotes the standard deviation, the value of which is presented in parentheses.

to be able to improve the CPP-CCSD results to be within 0.5 eV of the experimental values for Ne, CO, and H_2O,[61] it is formally a $O(N^7)$ method, which is outside the scope of this work.

As a larger test case, we also applied various energy-specific methods for calculation of the *K*-edge excitation of sulfur in dibenzothiophene (DBT; see Figure 2). We focus on the three

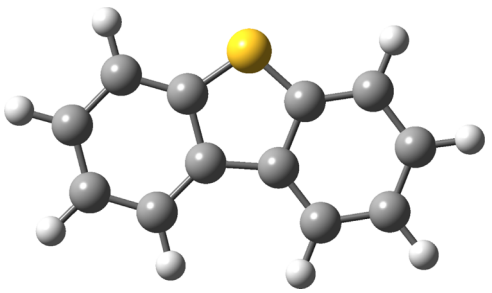

Figure 2. Structure of dibenzothiophene (DBT).

lowest $1s \rightarrow \pi$ excitation peaks, one (B2) at ∼2472 eV and two (B1 and A1) at ∼2474 eV, in the sulfur *K*-edge XAS spectrum of DBT.[82] Table 5 shows the calculated results obtained with different energy-specific methods. ES-EOM-CCSD and its perturbative approximations are consistent, and underestimate the sulfur *K*-edge excitations by no more than 1.7 eV compared to the experimental values. They show a small increase in absolute error compared to those for lighter elements (C, N, O). This increase in error is likely due to the neglect of relativistic corrections, as well as basis set incompleteness. The present calculations neglect relativistic effects. Neglecting relativistic effects leads to an underestimation in the computed spectra, and this error becomes larger as the atomic number increases. As a result, relativistic effect corrections are larger for sulfur than for light elements (C, N, O). It was estimated to be as large as ∼7 eV for the S 1s level.[82] On the other hand, basis set incompleteness overestimates the spectrum. For example, Fransson et al.[47] found that, for ethene and its fluoro derivatives, a red-shift of ∼1.3 eV must be applied to account for basis set incompleteness for a correlation consistent double-ζ basis set, and a red-shift of ∼0.5 eV for triple corrections for the CCSD method. The low-scaling approximations of EOM-CCSD are associated with a larger error, because of the basis set incompleteness. As a result, because of the error cancellation, P-EOM-MBPT2 happens to exhibit the best performance with the 6-311++G* basis, although this observation likely will not hold for larger basis sets.

For the *K*-edge excitation of sulfur, which is an element that is heavier than those previously studied, ES-TDDFT with the as-investigated two functionals, PBE1PBE and BHandHLYP, severely underestimate the excitations by ∼25−50 eV. Neither the relativistic effects nor the basis set incompleteness can explain the poor performance of TDDFT for sulfur *K*-edge excitation. Nevertheless, after the computed excitation energies are shifted so that the lowest XAS peak (B2) is aligned with the experimental value (2472 eV), all methods show an excellent agreement with the experiment for the second XAS peak ($1s \rightarrow 3p\sigma$), with ES-EOM-CCSD again being the best.

4. CONCLUSION

In this work, we presented a strategy using the low-scaling P-EOM-MBPT2 approach to improve the trial vectors for solving the EOM-CCSD equation with an emphasis on the high-energy excited states, e.g., core electron excitations. An energy-specific non-Hermitian Davidson eigensolver, facilitated by the energy-screening, eigenvector-bracketing, and growing window techniques, has been developed to efficiently obtain high-energy solutions without scanning through low-energy states. With these advances, EOM-CCSD and its low-scaling alternatives can be directly used to compute XAS. Applications to first-row

Table 5. Calculated S $1s \rightarrow \pi$ *K*-edge Excitation Energies for the Dibenzothiophene (DBT) Molecule[a]

	Absolute *K*-edge Excitation Energy (eV)			Shifted *K*-edge Excitation Energy (eV)	
	B2	B1	A1	B1	A1
experiment[82]	2472	2474	2474	2474	2474
ES-PBE1PBE	2420.55	2420.63	2422.26	2472.08	2473.71
ES-BHandHLYP	2446.19	2447.73	2448.69	2473.54	2474.50
ES-P-EOM-MBPT2	2471.29	2472.96	2473.35	2473.67	2474.06
ES-EOM-MBPT2	2470.38	2472.54	2472.68	2474.16	2474.30
ES-EOM-CCSD	2470.32	2472.42	2472.56	2474.10	2474.24

[a]The basis set used here is 6-311++G*.

DOI: 10.1021/acs.jctc.5b00459
J. Chem. Theory Comput. XXXX, XXX, XXX−XXX

elements (carbon, nitrogen, and oxygen) *K*-edge XAS of various modules show the wave-function-based methods (EOM-CCSD and its low-scaling alternatives) are not obviously advantageous, in terms of absolute excitations, compared to the spectra predicted by ES-TDDFT using the BHandHLYP functional. For *K*-edge XAS of heavier element, sulfur, EOM-CCSD and its low-scaling alternatives maintain the excellent performance while TDDFT severely underestimates the absolute excitation energies. After uniform spectral shift, all methods considered here perform very well for shifted *K*-edge XAS with ES-EOM-CCSD outperforming DFT and low-scaling alternatives in all statistical metrics.

■ ASSOCIATED CONTENT

Supporting Information

The Supporting Information is available free of charge on the ACS Publications website at DOI: 10.1021/acs.jctc.5b00459.

Calculated *K*-edge transition energies for some small molecules (PDF)

■ AUTHOR INFORMATION

Corresponding Author

*E-mail: xsli@uw.edu.

Notes

The authors declare no competing financial interest.

■ ACKNOWLEDGMENTS

The development of the ES-TDDFT method was funded by the U.S. National Science Foundation (No. CHE-1265945). The development and application of the ES-EOM-CCSD method and its low-scaling approximations to studies of X-ray absorption spectroscopy in this work is supported by the Ultrafast Initiative of the U.S. Department of Energy, Office of Science, Office of Basic Energy Sciences, through Argonne National Laboratory under Contract No. DE-AC02-06CH11357. PJL and JJG are grateful for the University of Washington Clean Energy Institute Graduate Fellowship (to P.J.L.) and the U.S. National Science Foundation Graduate Research Fellowship (No. DGE-1256082 to J.J.G.). Computations were facilitated through the use of advanced computational, storage, and networking infrastructure provided by the Hyak supercomputer system at the University of Washington, funded by the Student Technology Fee.

■ REFERENCES

(1) Stöhr, J. *NEXAFS Spectroscopy*; Springer−Verlag: Berlin, Heidelberg, Germany, 2003.
(2) Yannoulis, P.; Dudde, R.; Frank, K. H.; Koch, E. E. *Surf. Sci.* **1987**, *189-190*, 519−528.
(3) Aygül, U.; Batchelor, D.; Dettinger, U.; Yilmaz, S.; Allard, S.; Scherf, U.; Peisert, H.; Chassé, T. *J. Phys. Chem. C* **2012**, *116*, 4870−4874.
(4) Shadle, S. E.; Hedman, B.; Hodgson, K. O.; Solomon, E. I. *J. Am. Chem. Soc.* **1995**, *117*, 2259−2272.
(5) DuBois, J. L.; Mukherjee, P.; Stack, T. D. P.; Hedman, B.; Solomon, E. I.; Hodgson, K. O. *J. Am. Chem. Soc.* **2000**, *122*, 5775−5787.
(6) Chen, L. X.; Jäger, W. J.; Jennings, G.; Gosztola, D. J.; Munkholm, A.; Hessler, J. P. *Science* **2001**, *292*, 262−264.
(7) Casida, M. E. In *Recent Advances in Density Functional Methods (Part I)*; Chong, D. P., Ed.; World Scientific: Singapore, 1995; p 155.
(8) Stratmann, R. E.; Scuseria, G. E.; Frisch, M. J. *J. Chem. Phys.* **1998**, *109*, 8218−8224.
(9) Dreuw, A.; Head-Gordon, M. *Chem. Rev.* **2005**, *105*, 4009−4037.
(10) Stener, M.; Fronzoni, G.; de Simone, M. *Chem. Phys. Lett.* **2003**, *373*, 115−123.
(11) Ray, K.; DeBeer George, S.; Solomon, E. I.; Wieghardt, K.; Neese, F. *Chem.—Eur. J.* **2007**, *13*, 2783−2797.
(12) Besley, N. A.; Asmuruf, F. A. *Phys. Chem. Chem. Phys.* **2010**, *12*, 12024−12039.
(13) Lopata, K.; Van Kuiken, B. E.; Khalil, M.; Govind, N. *J. Chem. Theory Comput.* **2012**, *8*, 3284−3292.
(14) Liang, W.; Fischer, S. A.; Frisch, M. J.; Li, X. *J. Chem. Theory Comput.* **2011**, *7*, 3540−3547.
(15) Lestrange, P. J.; Nguyen, P. D.; Li, X. *J. Chem. Theory Comput.* **2015**, *11*, 2994−2999.
(16) Asmuruf, F. A.; Besley, N. A. *J. Chem. Phys.* **2008**, *129*, 064705.
(17) Bagus, P. S. *Phys. Rev.* **1965**, *139*, A619−A634.
(18) Slater, J. C.; Johnson, K. H. *Phys. Rev. B* **1972**, *5*, 844−853.
(19) Triguero, L.; Plashkevych, O.; Pettersson, L.; Ågren, H. *J. Electron Spectrosc. Relat. Phenom.* **1999**, *104*, 195−207.
(20) Evangelista, F. A.; Shushkov, P.; Tully, J. C. *J. Phys. Chem. A* **2013**, *117*, 7378−7392.
(21) Derricotte, W. D.; Evangelista, F. A. *Phys. Chem. Chem. Phys.* **2015**, *17*, 14360−14374.
(22) Song, J.-W.; Watson, M. A.; Nakata, A.; Hirao, K. *J. Chem. Phys.* **2008**, *129*, 184113.
(23) Besley, N. A.; Peach, M. J. G.; Tozer, D. J. *Phys. Chem. Chem. Phys.* **2009**, *11*, 10350−10358.
(24) Monkhorst, H. J. *Int. J. Quantum Chem.* **1977**, *12*, 421−432.
(25) Koch, H.; Jørgensen, P. *J. Chem. Phys.* **1990**, *93*, 3333−3344.
(26) Stanton, J. F.; Bartlett, R. J. *J. Chem. Phys.* **1993**, *98*, 7029−7039.
(27) Comeau, D. C.; Bartlett, R. J. *Chem. Phys. Lett.* **1993**, *207*, 414−423.
(28) Helgaker, T.; Coriani, S.; Jørgensen, P.; Kristensen, K.; Olsen, J.; Ruud, K. *Chem. Rev.* **2012**, *112*, 543−631.
(29) Shavitt, I.; Bartlett, R. J. *Many-Body Methods in Chemistry and Physics; MBPT and Coupled-Cluster Theory*; Cambridge University Press: Oxford, U.K., 2009.
(30) Stanton, J. F.; Gauss, J. *J. Chem. Phys.* **1995**, *103*, 1064−1076.
(31) Goings, J. J.; Caricato, M.; Frisch, M. J.; Li, X. *J. Chem. Phys.* **2014**, *141*, 164116.
(32) Gwaltney, S. R.; Nooijen, M.; Bartlett, R. J. *Chem. Phys. Lett.* **1996**, *248*, 189−198.
(33) Gwaltney, S. R.; Bartlett, R. J. *J. Chem. Phys.* **1999**, *110*, 62−71.
(34) Head-Gordon, M.; Oumi, M.; Maurice, D. *Mol. Phys.* **1999**, *96*, 593−602.
(35) Trofimov, A. B.; Schirmer, J. *J. Phys. B: At., Mol. Opt. Phys.* **1995**, *28*, 2299−2324.
(36) Trofimov, A. B.; Moskovskaya, T. E.; Gromov, E. V.; Vitkovskaya, N. M.; Schirmer, J. *J. Struct. Chem.* **2000**, *41*, 483−494.
(37) Plekan, O.; Feyer, V.; Richter, R.; Coreno, M.; de Simone, M.; Prince, K. C.; Trofimov, A. B.; Gromov, E. V.; Zaytseva, I. L.; Schirmer, J. *Chem. Phys.* **2008**, *347*, 360−375.
(38) Cederbaum, L. S.; Domcke, W.; Schirmer, J. *Phys. Rev. A: At., Mol., Opt. Phys.* **1980**, *22*, 206−222.
(39) Foresman, J. B.; Head-Gordon, M.; Pople, J. A.; Frisch, M. J. *J. Phys. Chem.* **1992**, *96*, 135−149.
(40) Head-Gordon, M.; Rico, R. J.; Oumi, M.; Lee, T. J. *Chem. Phys. Lett.* **1994**, *219*, 21−29.
(41) Asmuruf, F. A.; Besley, N. A. *Chem. Phys. Lett.* **2008**, *463*, 267−271.
(42) Nooijen, M.; Bartlett, R. J. *J. Chem. Phys.* **1995**, *102*, 6735−6756.
(43) Brabec, J.; Bhaskaran-Nair, K.; Govind, N.; Pittner, J.; Kowalski, K. *J. Chem. Phys.* **2012**, *137*, 171101.
(44) Sen, S.; Shee, A.; Mukherjee, D. *Mol. Phys.* **2013**, *111*, 2625−2639.
(45) Dutta, A. K.; Gupta, J.; Vaval, N.; Pal, S. *J. Chem. Theory Comput.* **2014**, *10*, 3656−3668.
(46) Coriani, S.; Fransson, T.; Christiansen, O.; Norman, P. *J. Chem. Theory Comput.* **2012**, *8*, 1616−1628.

DOI: 10.1021/acs.jctc.5b00459
J. Chem. Theory Comput. XXXX, XXX, XXX−XXX

(47) Fransson, T.; Coriani, S.; Christiansen, O.; Norman, P. *J. Chem. Phys.* **2013**, *138*, 124311.
(48) Kauczor, J.; Norman, P.; Christiansen, O.; Coriani, S. *J. Chem. Phys.* **2013**, *139*, 211102.
(49) Crawford, T. D.; Schaefer, H. *Rev. Comput. Chem.* **2000**, *14*, 33−136.
(50) Löwdin, P. O. *J. Mol. Spectrosc.* **1963**, *10*, 12−33.
(51) Davidson, E. R. *J. Comput. Phys.* **1975**, *17*, 87−94.
(52) Hirao, K.; Nakatsuji, H. *J. Comput. Phys.* **1982**, *45*, 246−254.
(53) Caricato, M.; Trucks, G. W.; Frisch, M. J. *J. Chem. Theory Comput.* **2010**, *6*, 1966−1970.
(54) Rettrup, S. *J. Comput. Phys.* **1982**, *45*, 100−107.
(55) Wang, Z.; Tu, Z.; Wang, F. *J. Chem. Theory Comput.* **2014**, *10*, 5567−5576.
(56) Frisch, M. J.; Trucks, G. W.; Schlegel, H. B.; Scuseria, G. E.; Robb, M. A.; Cheeseman, J. R.; Scalmani, G.; Barone, V.; Mennucci, B.; Petersson, G. A.; Nakatsuji, H.; Caricato, M.; Li, X.; Hratchian, H. P.; Izmaylov, A. F.; Bloino, J.; Zheng, G.; Sonnenberg, J. L.; Liang, W.; Hada, M.; Ehara, M.; Toyota, K.; Fukuda, R.; Hasegawa, J.; Ishida, M.; Nakajima, T.; Honda, Y.; Kitao, O.; Nakai, H.; Vreven, T.; J. A. Montgomery, J.; Peralta, J. E.; Ogliaro, F.; Bearpark, M.; Heyd, J. J.; Brothers, E.; Kudin, K. N.; Staroverov, V. N.; Keith, T.; Kobayashi, R.; Normand, J.; Raghavachari, K.; Rendell, A.; Burant, J. C.; Iyengar, S. S.; Tomasi, J.; Cossi, M.; Rega, N.; Millam, J. M.; Klene, M.; Knox, J. E.; Cross, J. B.; Bakken, V.; Adamo, C.; Jaramillo, J.; Gomperts, R.; Stratmann, R. E.; Yazyev, O.; Austin, A. J.; Cammi, R.; Pomelli, C.; Ochterski, J. W.; Martin, R. L.; Morokuma, K.; Zakrzewski, V. G.; Voth, G. A.; Salvador, P.; Dannenberg, J. J.; Dapprich, S.; Parandekar, P. V.; Mayhall, N. J.; Daniels, A. D.; Farkas, O.; Foresman, J. B.; Ortiz, J. V.; Cioslowski, J.; Fox, D. J. *Gaussian Development Version, Revision H.36*; Gaussian, Inc.: Wallingford, CT, 2014.
(57) Weigend, F.; Ahlrichs, R. *Phys. Chem. Chem. Phys.* **2005**, *7*, 3297−3305.
(58) Rappoport, D.; Furche, F. *J. Chem. Phys.* **2010**, *133*, 134105.
(59) Feller, D. *J. Comput. Chem.* **1996**, *17*, 1571−1586.
(60) Schuchardt, K. L.; Didier, B. T.; Elsethagen, T.; Sun, L.; Gurumoorthi, V.; Chase, J.; Li, J.; Windus, T. L. *J. Chem. Inf. Model.* **2007**, *47*, 1045−1052.
(61) Coriani, S.; Christiansen, O.; Fransson, T.; Norman, P. *Phys. Rev. A: At., Mol., Opt. Phys.* **2012**, *85*, 022507.
(62) Schirmer, J.; Trofimov, A. B.; Randall, K. J.; Feldhaus, J.; Bradshaw, A. M.; Ma, Y.; Chen, C. T.; Sette, F. *Phys. Rev. A: At., Mol., Opt. Phys.* **1993**, *47*, 1136−1147.
(63) Bartlett, R. J.; Stanton, J. F. *Rev. Comput. Chem.* **1994**, *5*, 65−169.
(64) Rittby, M.; Bartlett, R. J. *J. Phys. Chem.* **1988**, *92*, 3033−3036.
(65) Stanton, J. F.; Gauss, J.; Bartlett, R. J. *J. Chem. Phys.* **1992**, *97*, 5554−5559.
(66) Tronc, M.; King, G. C.; Read, F. H. *J. Phys. B: At. Mol. Phys.* **1979**, *12*, 137−157.
(67) Hitchcock, A. P.; Brion, C. E. *J. Electron Spectrosc. Relat. Phenom.* **1980**, *18*, 1−21.
(68) Ma, Y.; Chen, C. T.; Meigs, G.; Randall, K.; Sette, F. *Phys. Rev. A: At., Mol., Opt. Phys.* **1991**, *44*, 1848−1858.
(69) Tronc, M.; King, G. C.; Read, F. H. *J. Phys. B: At. Mol. Phys.* **1980**, *13*, 999−1008.
(70) Remmers, G.; Domke, M.; Puschmann, A.; Mandel, T.; Xue, C.; Kaindl, G.; Hudson, E.; Shirley, D. A. *Phys. Rev. A: At., Mol., Opt. Phys.* **1992**, *46*, 3935−3944.
(71) Domke, M.; Xue, C.; Puschmann, A.; Mandel, T.; Hudson, E.; Shirley, D. A.; Kaindl, G. *Chem. Phys. Lett.* **1990**, *173*, 122−128.
(72) Püttner, R.; Dominguez, I.; Morgan, T. J.; Cisneros, C.; Fink, R. F.; Rotenberg, E.; Warwick, T.; Domke, M.; Kaindl, G.; Schlachter, A. S. *Phys. Rev. A: At., Mol., Opt. Phys.* **1999**, *59*, 3415−3423.
(73) Shigemasa, E.; Ueda, K.; Sato, Y.; Sasaki, T.; Yagishita, A. *Phys. Rev. A: At., Mol., Opt. Phys.* **1992**, *45*, 2915−2921.
(74) Adachi, J.; Kosugi, N.; Shigemasa, E.; Yagishita, A. *J. Chem. Phys.* **1995**, *102*, 7369−7376.
(75) Becke, A. D. *J. Chem. Phys.* **1993**, *98*, 1372−1377.
(76) Adamo, C.; Barone, V. *J. Chem. Phys.* **1999**, *110*, 6158−6170.
(77) Perdew, J. P.; Burke, K.; Ernzerhof, M. *Phys. Rev. Lett.* **1996**, *77*, 3865−3868.
(78) Woon, D. E.; Dunning, T. H. *J. Chem. Phys.* **1994**, *100*, 2975−2988.
(79) Woon, D. E.; Dunning, T. H. *J. Chem. Phys.* **1995**, *103*, 4572−4585.
(80) DeBeer George, S.; Petrenko, T.; Neese, F. *Inorg. Chim. Acta* **2008**, *361*, 965−972.
(81) Fronzoni, G.; De Francesco, R.; Stener, M. *J. Phys. Chem. B* **2005**, *109*, 10332−10340.
(82) Mijovilovich, A.; Pettersson, L. G. M.; Mangold, S.; Janousch, M.; Susini, J.; Salome, M.; de Groot, F. M. F.; Weckhuysen, B. M. *J. Phys. Chem. A* **2009**, *113*, 2750−2756.

DOI: 10.1021/acs.jctc.5b00459
J. Chem. Theory Comput. XXXX, XXX, XXX−XXX